CHAPTER 6

CYCLIC TRIAXIAL TEST AND EICP STABILIZATION

6.1 General

Solidification / Stabilization with addition of cement-based binders is a substantiated treatment technique for soil contaminated with inorganic compounds. (Conner, 1993) whereas its application to organic compounds, in particular petroleum hydrocarbons, has a relatively limited experience. Several binders such as lime (Ochepo et al. 2013), lime-activated slag (Kogbara et al 2011, Kogbara and Al-Tabbaa, 2011), cement (Akinwumi et al. 2016), Rice-husk ash (Oluwatuyi and Ojuri 2014), Flyash (George et al. 2014, Shah et al. 2003), Bioaugmentation (Kogbara et al. 2016) and quicklime (Schifano et al. 2007) have been reportedly used specifically for stabilization of oil contaminated soils. Microbially induced calcite precipitate (MICP) is a trending technique that has gained a great deal of attention from researchers (DeJong et al. 2006; Whiffin et al. 2007; van Passen et al. 2010; Chu et al. 2012; Montoya and DeJong 2015). Nonetheless, relying on bacteria as the source of urease enzyme for MICP poses several nonentities and ambiguities (e.g., availability of oxygen, presence of other microorganisms, physical non-homogeneity and complex pore fluid chemistry) which may raise complexities (Almajed et al. 2018). Enzymatically induced calcite precipitate (EICP) has been recommended as a means of addressing some of the challenges of enhancing the geotechnical properties of soil by substituting the use of bacterial cells with enzyme as the source of urease. (Hamdan et al. 2013). Several researchers have

studied EICP for soil improvement purposes (Yasuhara et al. 2012, Zhao et al. 2016, Putra et al. 2017a) but only a handful of research has been conducted on the cyclic behavior of EICP treated soil (Simatupang et al. 2018). Indeed, in the author's knowledge, no work till now has been conducted to examine the efficiency of EICP to stabilize hydrocarbon contaminated soils.

Based on the current state of knowledge, the main theme of this chapter is to upscale the EICP technique in stabilization of hydrocarbon contaminated sands. The efficiency of the technique was evaluated in terms of cyclic pore pressure and modulus degradation. Prior to that, a supporting analysis to study the effect of crude oil contamination on the cyclic response of sand has also been presented.

6.2 Test procedures and Conditions

6.2.1 Chemicals

The reagent-grade calcium chloride dihydrate and urea (≥99) were used for preparing EICP solution. Jack beans urease enzyme powder with a reported activity of 3500 units/g at room temperature was also purchased from CDH Chemicals. To induce cementation with EICP, a mix of enzyme and cementation solution of urea and calcium chloride of "preferred concentration" was used. The preferred concentration was determined by conducting falcon tube tests.

6.2.2 Falcon Tube Tests

To investigate the effect of constituent chemicals used in EICP solution on the efficiency of carbonate precipitate and determine the *preferred concentration,* a series of 12 precipitation tests were carried out in falcon tubes. The preferred concentration here refers to that concentration of constituent chemicals will yield both high precipitation mass and high

precipitation efficiency. It is measured in terms of precipitation ratio which is defined as the ratio of measured precipitation mass ($W_{experimental}$) to the theoretical maximum precipitate based upon the amount of calcium in EICP solution ($W_{theoritical}$). Mathematically, it can be expressed by eq. (6.1).

$$\text{Precipitation ratio} = \frac{W_{experimental}}{W_{theoritical}} \tag{6.1}$$

Tests were conducted in a 50-mL test tubes containing 20 mL of EICP solution without any soil shown in Fig 6.1(a). Based on concentrations of the EICP solution used in previous research (Almajed 2019, Carmona et al. 2016, Zhao et al. 2016) the concentration of urea ranged from 0.25 to 1.0 M, the ratio of $CaCl_2$ to urea varied from 1:1 to 1:1.75, and the enzyme concentration ranged between 3 to 6 g/L. To prepare EICP solution, calcium chloride and urea were first dissolved into deionized water and then free urease enzyme was added. The test tubes were kept aside for incubation periods of 7, 14 and 21 days with periodic shakings. Following the respective incubation period, the precipitate in the tubes were collected using ashless filter paper. Fig 6.1(b) shows the collected precipitate after thoroughly rinsing with deionized water and oven dried for 24h at 50°C. Afterward, the mass of the dried precipitates that remained on the filter paper was measured.

Fig. 6.1 (a) Falcon tubes containing EICP solution (b) Filter papers containing calcite precipitate

Table 6.1 presents the average value of the concentrations of constituents for each of the 12 cases and the corresponding precipitation ratio achieved after an incubation period of 7 days, 14 days and 21 days. Each test was repeated thrice to check the reproducibility of the procedure and their average value was considered. It can be clearly observed from the results that the maximum precipitation ratio was observed for urea concentration 1M, $CaCl_2$ 0.67M, Urea:$CaCl_2$ ratio of 1:1.5 with enzyme 5g/L. On the basis of these tests in support with the investigations conducted by Almajed et al. (2018), these concentrations were selected as the preferred concentrations in the further study.

Table 6.1 Summary of tube tests

Test No.	Urea (M)	$CaCl_2$ (M)	Urea:$CaCl_2$	Enzyme (g/L)	Precipitation Ratio		
					7 days incubation	14 days incubation	21 days incubation
1.	1.0	1.0	1:1	3.0	0.60	0.82	1.0
2.	0.5	0.5	1:1	3.0	0.74	0.94	1.0
3.	0.25	0.25	1:1	3.0	0.68	0.85	1.0
4.	0.61	0.41	1:1.5	3.0	0.80	0.91	0.92
5.	1.0	0.67	1:1.5	3.0	0.87	0.91	0.95
6.	1.0	0.67	1:1.5	5.0	0.96	1.0	1.0
7.	0.61	0.35	1:1.75	5.0	0.89	0.97	1.0
8.	1.0	0.57	1:1.75	3.0	0.93	0.88	0.93
9.	1.0	0.57	1:1.75	5.0	0.90	0.97	1.0
10.	1.0	0.83	1:1.2	6.0	0.98	0.96	0.97
11.	1.0	0.83	1:1.2	5.0	0.92	0.91	1.0
12.	1.0	0.83	1:1.2	3.0	0.84	0.90	0.845

6.2.3 Specimen Preparation

The experimental work is focused on investigating the effect of EICP on cyclic pore pressure and cyclic shear modulus of hydrocarbon contaminated Guwahati sand through strain-controlled cyclic triaxial test. The tests were conducted in three series. In the first series, crude oil contaminated sand without EICP treatment were tested. In the second series, clean

and contaminated sand specimens subjected to 7 days EICP curing were tested. Finally, in third phase, sand specimens subjected to 14 days EICP curing were tested.

To prepare contaminated sand for further preparing the triaxial samples, the sand was first oven-dried so as to completely remove any existing moisture traces. It was then uniformly mixed with crude oil at varying oil dosages of 2, 4, 6, 8, and 10% (volume by weight) and kept in sealed bags for one week to allow proper interaction of oil and soil. The above mentioned range of crude oil dosage was selected as per the basis of previous literature (Al-Sanad et al. 1995; Khamehchiyan 2007; Taqieddin 2017). Both dry and quasi-moist tamping methods were employed for preparing the clean and contaminated samples respectively. Quasi-moist tamping method for preparation of contaminated samples involved mixing of the oven-dried sand with calculated amount of crude oil after which the moist sand was deposited into a cylindrical split mold (dia 50mm) and compacted in 5 layers. Each layer was compacted using a small tamper. The number of blows applied for each layer was carefully controlled. In order to achieve sample uniformity and desired relative density ($D_r \approx 50\%$), undercompaction technique proposed by Ladd (1978) was employed. For each layer, the compactive effort was increased towards the top with the undercompaction ratio of 2.5 %. Additionally, a suction of 20kPa was employed to hold the sample vertically. After attaining the desired height (10cm) and void ratio, the split sampler was removed.

For preparing EICP treated specimens, hand mixing of EICP solution and enzyme powder into the clean and contaminated sand was preferred rather than using permeation grouting of the solution as the latter is very sensitive and difficult to control (Persoff et al.1999). Due to better control, former method therefore also ensures maximized reproducibility of the samples. Urea and $CaCl_2$ solutions with preferred concentrations of 1M and 0.67M

respectively were mixed in the ratio of 1:1.5 resulting in the total solution volume corresponding to the OMC of the Guwahati sand. This solution along with powdered enzyme weighing equivalent to 5g/l was mixed with the pre-calculated amount of sand. The mixture was then compacted into the mold in 5 layers and extracted through an extruder. The specimens were cured for 7 and 14 days inside chamber with controlled humidity (50±5%) and temperature (38±2ºC).

6.2.4 Testing program

A series of 36 undrained cyclic triaxial tests were executed in this research according to ASTM D 3999. Table 6.2 presents a summary of the main characteristics of tests conducted in this study.

Table 6.2. Summary of cyclic triaxial tests conducted at σ_c = 1.0 kg/cm^2 and void ratio, e = 0.749

S.No	Sand Type	Curing Period	Cyclic Shear Strain, γ (%)	Oil content, ω (%)
1.	Untreated	-	0.5	0, 2, 4, 6, 8, 10
			1.0	0, 2, 4, 6, 8, 10
2.	EICP treated	7 Days	0.5	0, 2, 4, 6, 8, 10
			1.0	0, 2, 4, 6, 8, 10
		14 Days	0.5	0, 2, 4, 6, 8, 10
			1.0	0, 2, 4, 6, 8, 10

The cyclic triaxial apparatus is unidirectional with variable amplitude and frequency that can be adjusted as per the test requirements. Fig. 6.2 shows the photographic representation of cyclic triaxial set up which mainly consists of a pneumatic actuator for load application, triaxial cell and pressure controllers for applying cell pressure and back pressure. The tests conducted in this study are strain-controlled with cyclic strain amplitude (γ) = 0.5mm and 1mm and loading frequency of 1Hz (Fig.6.3).

The specimens for cyclic triaxial tests were saturated by applying back pressure until the Skempton's pore pressure parameter (B) is greater than or equal to 0.95. Specimens are then isotropically consolidated under an effective confining stress (σ_c') = 100kPa. Undrained conditions were chosen to simulate dynamic earthquake loading in the field (Huang and Wang 2016). The results were recorded in terms of normalized pore fluid pressure (r_u) and secant shear modulus (G). The test was terminated after 100 loading cycles and the r_u values reached at the end of 100^{th} cycle was recorded in each case for comparison.

Fig. 6.2 Experimental setup for cyclic triaxial system

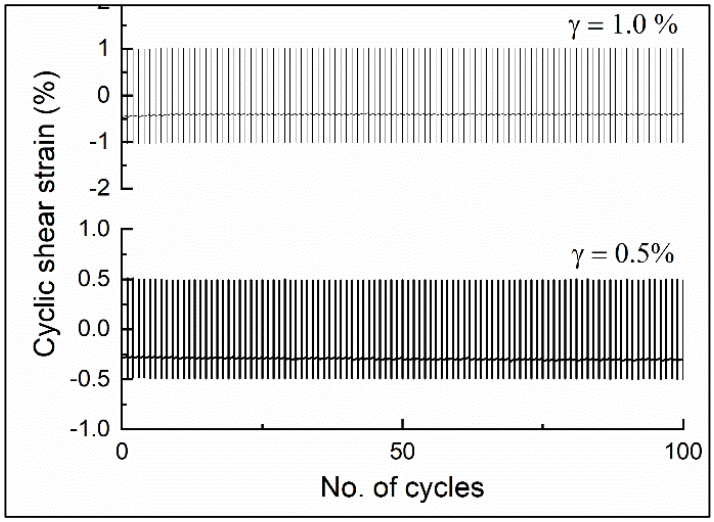

Fig. 6.3 Applied cyclic shear strain versus number of cycles

6.3 Experimental Results and Discussions

6.3.1 Pore Pressure Response of Hydrocarbon Contaminated Guwahati Sand

A series of strain-controlled undrained cyclic triaxial tests were conducted on crude oil contaminated Guwahati sand with varying percentages of crude oil, ω, (0, 2, 4, 6, 8 and 10%) subjected to a sinusoidal loading of frequency 1 Hz at two different cyclic shear strain amplitudes (0.5mm and 1mm). Typical results of the cyclic test conducted on sand with ω = 2%, targeting a skeleton relative density of approximately 50%, isotropically consolidated to 1.0 kg/cm^2 subjected to 100 loading cycles of frequency 1Hz and cyclic shear strain of 1.0% are shown in Fig 6.4. Fig. 6.4(a) shows the variation of deviatoric stress with the cyclic shear strain. The hysteresis loop became flatter with each applied loading cycles which indicates loss of cyclic strength due to building up of excess pore pressure. Fig. 6.4(b) exhibits the evolution of the deviatoric stress with the number of cycles. Fig 6.4(c) is a plot between mean effective stress and deviatoric stress showing the effective stress path followed by the specimen. The movement of stress path from left to right is attributed to the reduction in the effective confining pressure with the development of excess pore pressure. Fig. 6.4(d) is a

plot of effective confining stress with the number of cycles. Fig 6.4(d) indicates that there was a sudden rise of excess pore pressure in the initial few cycles. The effective confining stress decreased rapidly in first 10 cycles; afterwards, the effective confining stress decreased steadily until about 50 cycle. At this point, an initiation of liquefaction phenomenon was observed. In this study, point of liquefaction initiation has been defined as the point where r_u attains a value of 0.9. Full liquefaction state is said to be achieved when r_u equals 1.0. It is evident from the figures that when 2% crude oil contaminated sand was subjected to 100 loading cycles at γ=0.5%, there seems to be an initiation of liquefaction stage but yet full liquefaction state was not achieved.

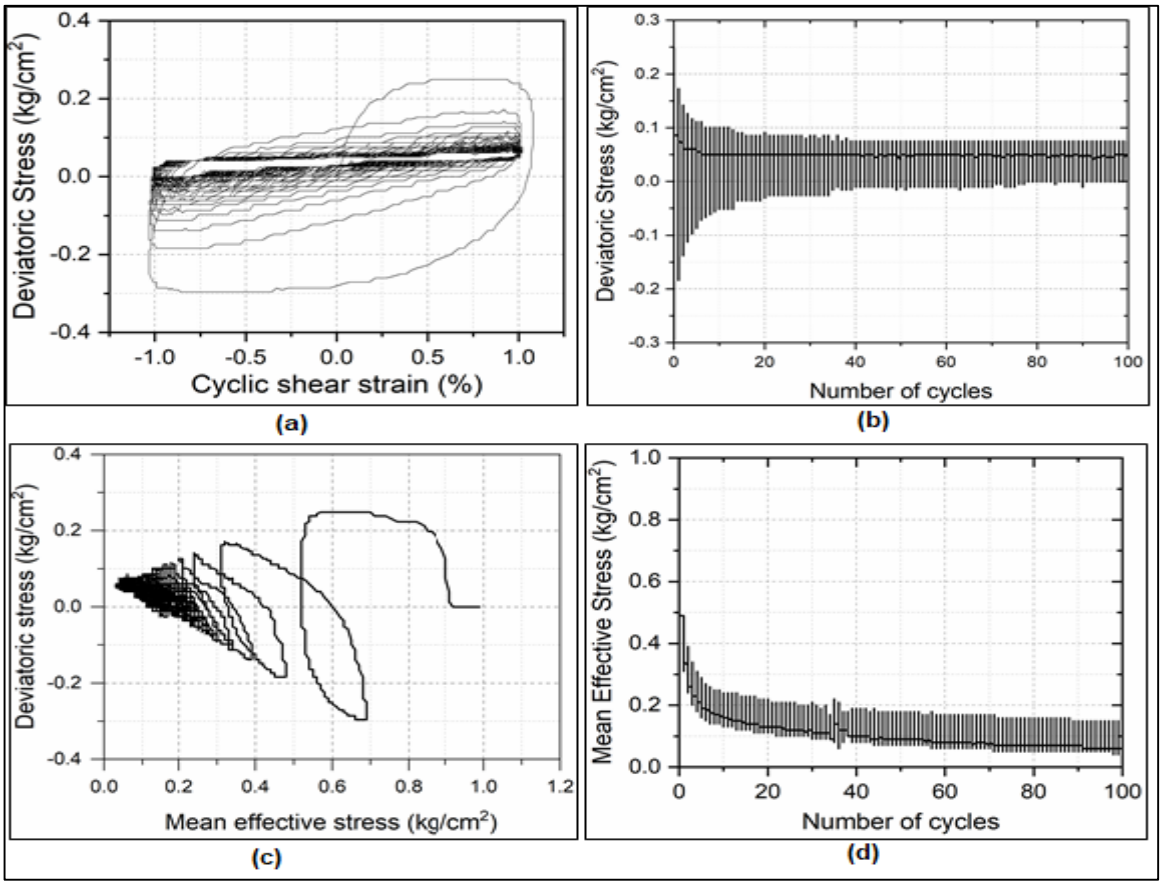

Fig. 6.4 Results of strain-controlled cyclic test for ω= 2%, σ_c = 1.0kg/cm², γ= 1.0% (a) deviatoric stress with cyclic shear strain; (b) deviatoric stress with no. of cycles; (c) effective stress path; (d) mean effective stress with number of cycles

Presence of hydrocarbon compounds in the soil matrix has a significant effect on the development of cyclic pore pressure by altering the physio-chemical properties of sand as well as pore fluid. Oil contamination also transforms the soil-water characteristic curve (SWCC) by changing the matric suction values. However, this particular aspect has not been considered here, as all the tests in this study has been conducted at fully saturated state where the matric suction is negligible. Fig. 6.5 and Fig. 6.6 presents the pore pressure response of Guwahati sand contaminated with varying percentages of crude oil at γ = 0.5% and 1.0% respectively. In the figures, small red arrow marks the instant at which the liquefaction initiates (i.e. r_u = 0.9) or the maximum value of pore pressure ratio, $r_{u,\,max}$, attained in 100 cycles, whichever occurs first.

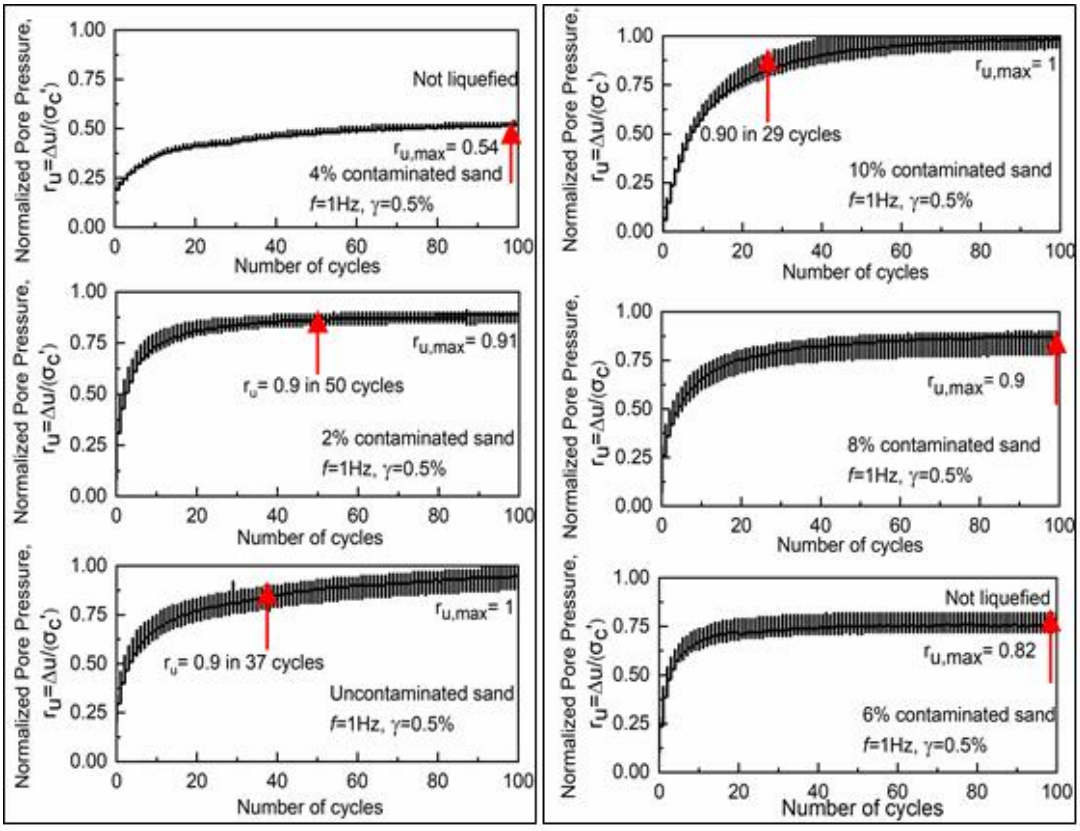

Fig. 6.5 Normalized cyclic pore pressure response of crude oil contaminated Guwahati sand at γ = 0.5%, σ_c = 1.0 kg/cm^2

For ω = 0% i.e. uncontaminated sand, and γ = 0.5%, liquefaction was initiated in 37 loading cycles while the value of $r_{u, max}$ reached after 100 loading cycles was 1. It implies that the sand was in full liquefied state at the end of 100^{th} cycles. The maximum value of $r_{u, max}$ observed for ω = 4% and 6% at γ= 0.5% was 0.54 and 0.82 respectively. The value of $r_{u, max}$ starts increasing when ω increases beyond 4%. It was also observed that the number of cycles required for liquefaction initiation increased with initial increment in crude oil content meaning thereby, the liquefaction resistance initially increased with increasing crude oil content. Indeed, there were no signs of liquefaction for 4% and 6% contaminated sands even after applying 100 loading cycles. Where the signs of liquefaction were absent for 4% and 6% contaminated sands, 8% contaminated sand showed some signs of liquefaction while nearing 100^{th} cycle. The liquefaction resistance for 10% contaminated sand dropped even below that of virgin sand.

Fig 6.6 shows the development of cyclic pore pressure with the loading cycles in crude oil contaminated sand at γ =1.0%. In this case, initiation of liquefaction was evident for all percentages of crude oil contamination. Maximum pore pressure ratio observed after 100 cycles showed a reducing trend upto ω = 6% after which it again starts increasing. This observation was slightly deviated with the one observed at γ = 0.5%, where such a transition was observed at ω = 4% only. However, the number of cycles required to reach r_u= 0.9 was 43 for ω = 4% while it was 41 for ω = 6%. Hence it can be inferred from both the figures that there is a transition point in terms of crude oil content upto which the liquefaction resistance increases. Addition of crude oil beyond this point causes the liquefaction resistance to fall off sharply. Hence the variation of $r_{u,max}$ with crude oil content results into a v-shaped profile with the lowest value observed at ω = 4% (Fig. 6.10). Hence it can be stated that initial

contamination with crude oil moderately enhances the liquefaction resistance which then degrades with higher percentages of contamination.

There can be two underlying mechanism which can explain such a transition. The first mechanism owes to the difference in the bulk modulus of the pore fluids which is dominant at lower oil contents. At lower degrees of contamination, the amount of crude oil is insufficient to completely coat the sand grains and it occupies the inter-granular voids in the form of oil droplets as can be seen from the SEM images in Fig. 6.9(a) and 6.9(b).

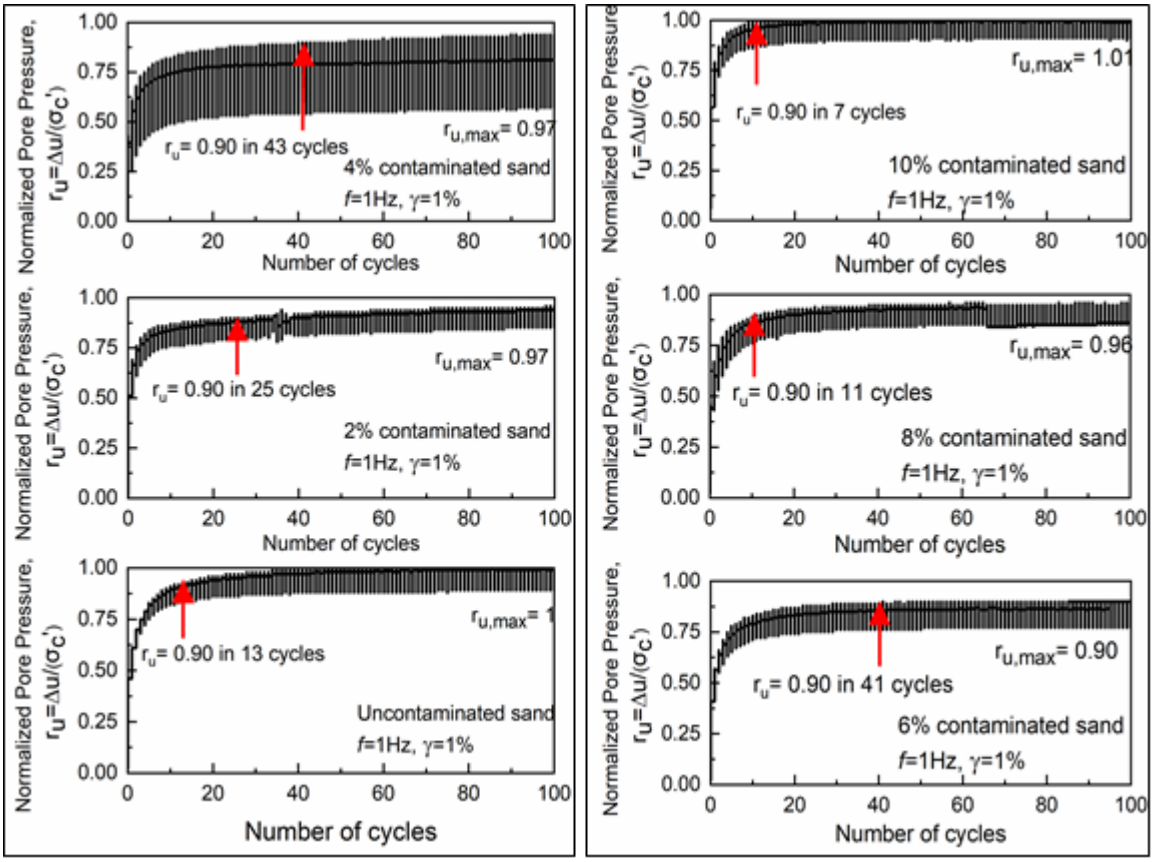

Fig. 6.6 Normalized cyclic pore pressure response of crude oil contaminated Guwahati sand at $\gamma = 0.5\%$, $\sigma_c = 1.0$ kg/cm^2

Consequently, the grain to grain contact still exists and there appears to be negligible loss of effective stress. Moreover, it is also evident from the previous studies (Khamehchiyan et al.

2007) that oil contamination induces an apparent cohesion due to pore-fluid viscosity which will again be helpful in holding the soil matrix intact. The pore fluid pressure generation in such a case would be from the combined effect of oil and water. Since the bulk modulus of oil is lower than that of water, the pressure generated by oil would be lesser than water. This explains the reduction in the pore pressure and hence increase in liquefaction resistance with initial contamination i.e., up to ω = 4%. The second mechanism explains the behavior observed beyond ω = 4%. At higher degrees of contamination, the sand grains get completely smeared with a hydrocarbon layer and fill the micro and macro pores of the soil as well. Consequently, it can effectively decompose the inter-particle contact friction and majority of soil grains would lose their contacts with neighboring grains. Moreover, the effective stress resulting from the grain-to-grain contact surface also gets lost which in turn reduces the liquefaction resistance. Hence it can be inferred that at lower oil content compressibility characteristics of pore fluid dominates while at higher oil content frictional characteristics of sand grains dominates.

6.3.2 Pore Pressure Response of EICP treated Hydrocarbon Contaminated Sand

To examine the potential influence of EICP technique in improving the cyclic response of crude oil contaminated Guwahati sand, undrained triaxial tests were carried out on contaminated samples subjected to EICP treatment with a curing period of 7 days and 14 days. The observed pore pressure profiles for treated samples have been compared with the untreated ones at both γ = 0.5% and 1.0%. Fig. 6.7and Fig. 6.8 shows the normalized excess pore pressure profiles of clean and contaminated sand before and after EICP treatment for different oil content and curing periods for γ= 0.5% and γ=1.0% respectively.

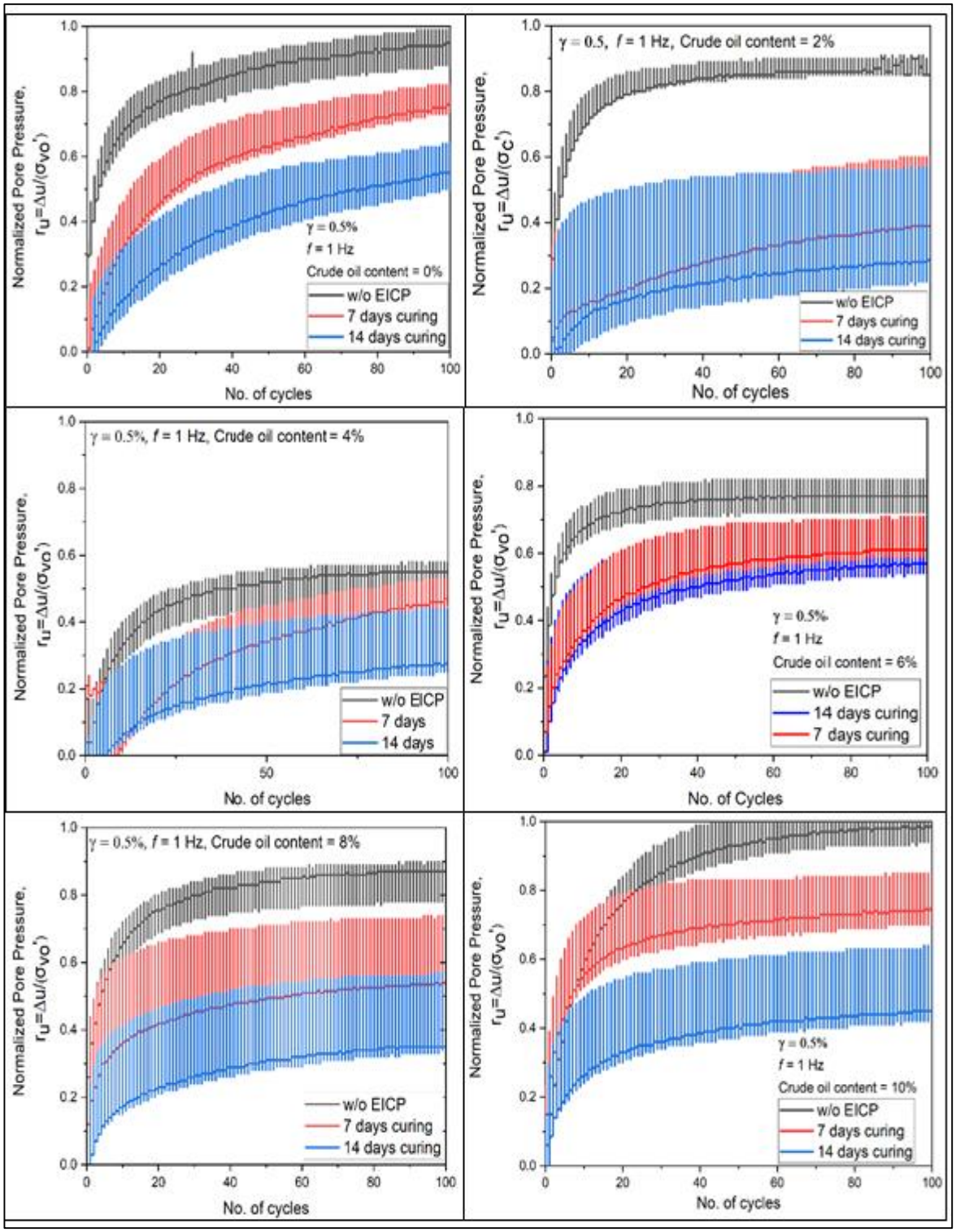

Fig. 6.7 Normalized cyclic pore pressure response of EICP treated sand specimens for different crude oil content at γ = 0.5%

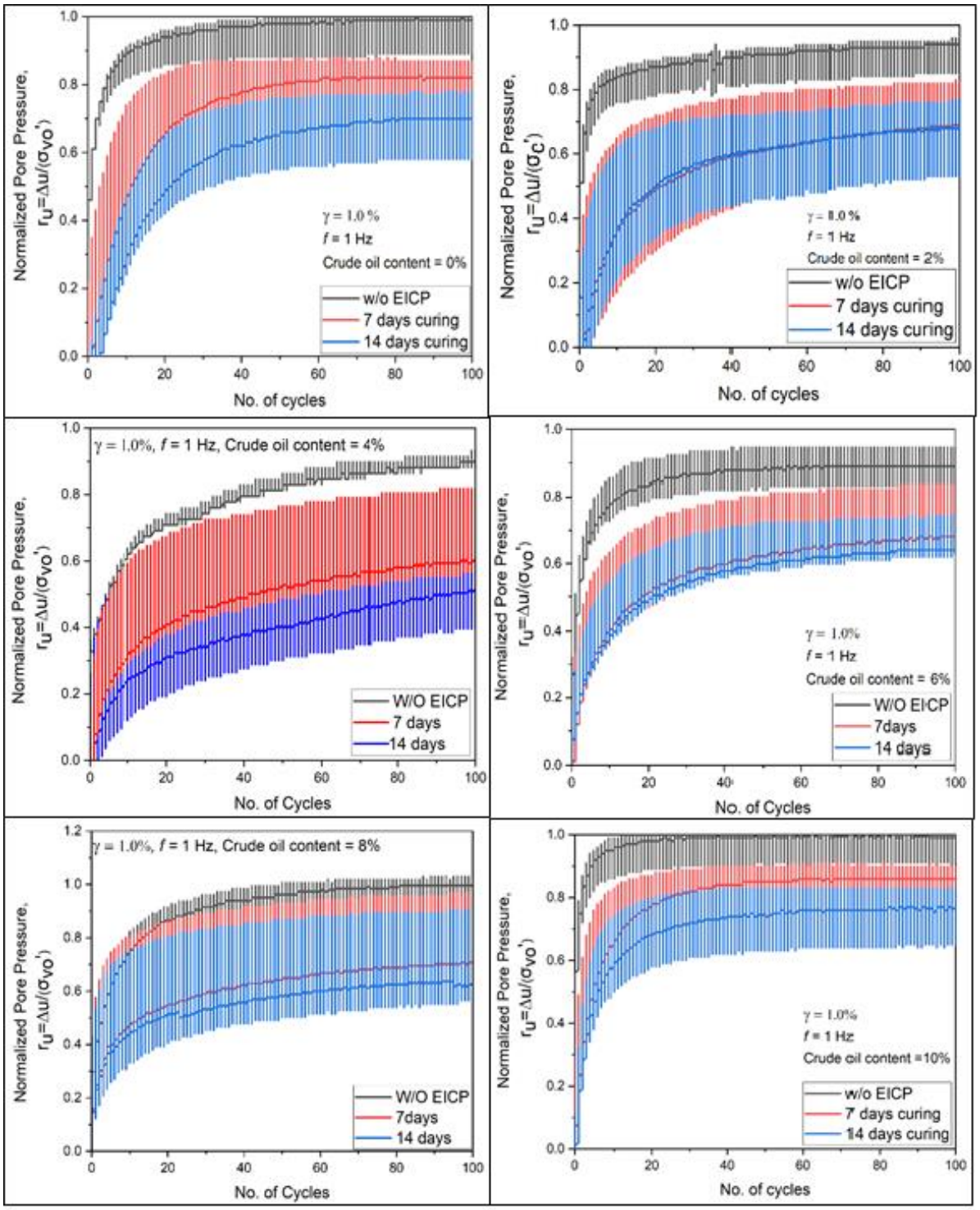

Fig. 6.8 Normalized cyclic pore pressure response of EICP treated sand specimens for different crude oil content at γ = 1.0%

. It is apparent from the figures that cementation through calcite precipitation reduces the levels of excess pore pressure ratio. The value of $r_{u, max}$ after application of 100 loading cycles at $\gamma = 0.5\%$ for uncontaminated sand without EICP was 1.0 while the same after subjecting to 7 days and 14 days EICP treatment attains $r_{u, max}$ equals to 0.82 and 0.64 respectively. Similarly, it can be seen that for $\omega = 2\%$, value of $r_{u, max}$ dropped from 0.90 to 0.60 after 7 days curing period and from 0.6 to 0.57 after 14 days curing period. It can also be observed that for $\omega = 0\%$, the rate of building up of excess pore pressure is slower for 7 days cured specimens and even more slower for 14 days cured specimens as compared with the untreated specimens. However, in case of contaminated sands, this rate was not significantly improvised by the EICP treatment in considered range of cyclic strains.

Fig. 6.8 shows the normalized pore pressure response for EICP treated clean and contaminated sand for different curing periods at $\gamma = 1.0\%$. Again, the calcite-precipitated sand has lower values of pore pressure ratio than the untreated sand for all values of ω. The difference in the pore pressure ratios after 7 days curing and 14 days curing was smaller as compared to the untreated and 7 days cured specimens. Similar trend was also evident in the results obtained for $\gamma = 0.5\%$. Therefore, this particular observation indicates that a major fraction of total calcite precipitation was achieved during the first 7 days itself.

To elucidate the principal mechanism through which enzyme-induced bio-cemented sand offers a greater cyclic resistance, SEM analyses were conducted. Fig. 6.9 (c) and 6.9 (d) shows the SEM image of 14 days cured uncontaminated EICP treated specimen respectively. The precipitation of the calcite crystals was visually evident at three locations namely, (i) inter-particle contact points, (ii) on the surrounding sand surface area and (iii) within the internal pore space. Such a pattern of crystal deposition binds the sand particles together and

contributes to soil strengthening. The cyclic response of the sand is stiffer and the generated excess pore pressure remains low. Also, precipitated calcite crystals occupies void spaces which reduces the matrix permeability and subsequently liquefaction potential is reduced (Hoang et al. 2020).

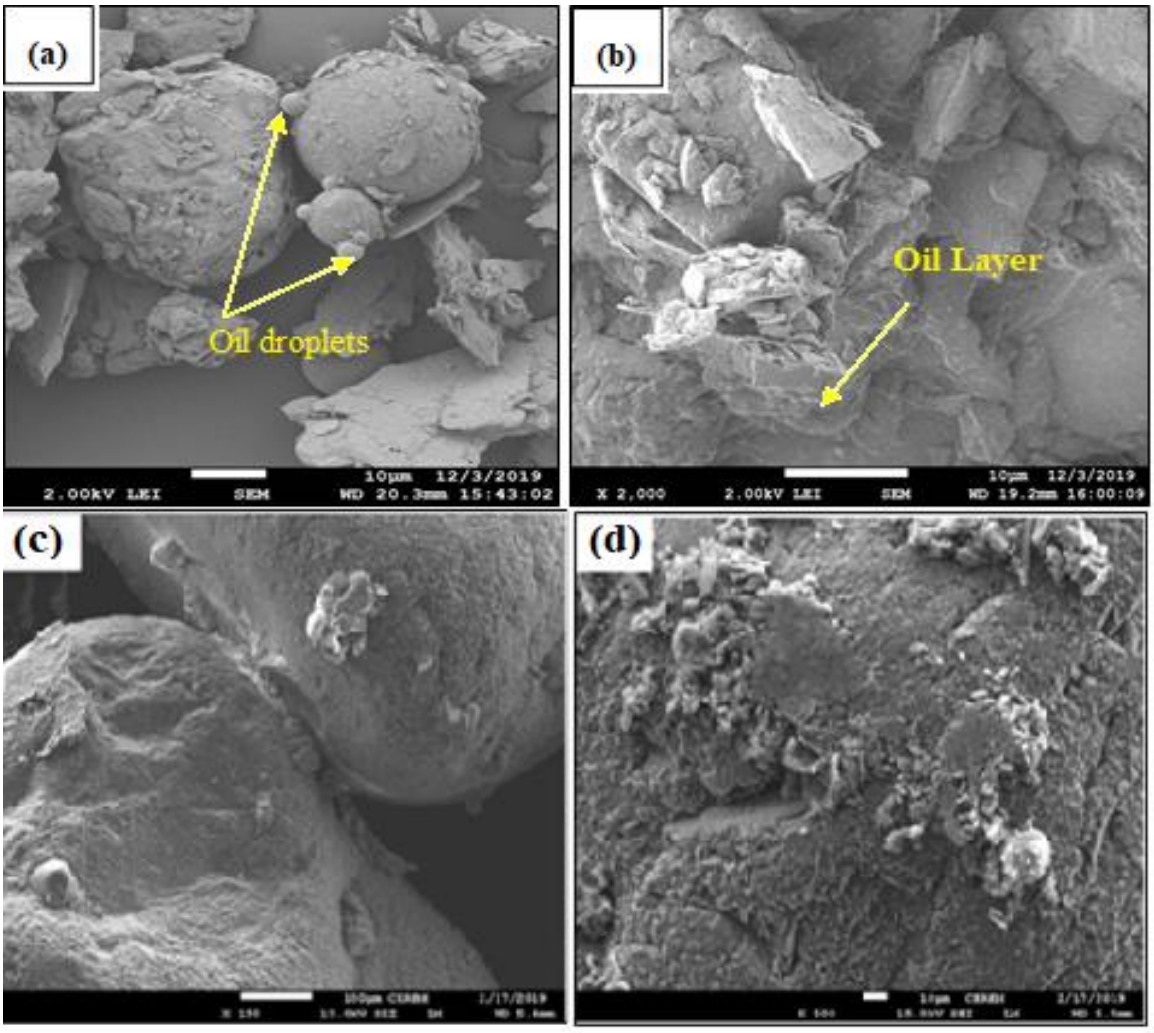

Fig. 6.9 SEM images of untreated sand (a) at ω = 4%, (b) ω = 8% and EICP uncontaminated sand exhibiting cementation (c) at grain to grain contact surface and (d) on the sand grain surface

It is worth noticing that the percentage change in $r_{u,max}$ for untreated specimens (both contaminated and uncontaminated) was higher for γ = 0.5%. For 10% contaminated samples and γ = 0.5%, the observed percentage change in $r_{u,\ max}$ for 7 days and 14 days cured

specimens is 16% and 25% respectively. On the other hand, for the same degree of contamination and γ = 1.0%, the observed percentage change in $r_{u,\,max}$ for 7 days and 14 days cured specimens is 8% and 10% respectively. Hence it is possible to generate dual inference from the above results. Firstly, the observed patterns of the excess pore pressure levels at two different cyclic strains indicates that the efficiency of the EICP treatment diminish at higher levels of cyclic strains (Vucetic and Mortezaie 2015). And secondly, the variation of rate of generation of excess pore pressure with crude oil content indicates that the efficiency of calcite-precipitation reduces at higher levels of crude oil contents.

The reduction in the efficiency of EICP with increasing crude oil content can have multiple possible explanations. It has been reported that the increasing oil content has negative influence on the activity of the urease enzyme (Wyszkowska et al. 2002). The presence of hydrocarbon compounds slows down the reaction between urea-$CaCl_2$ and urease enzyme thereby inhibiting the formation of calcite precipitate. Also, crude oil contamination may lead to reduced specific surface area providing lesser particle contacts for inter-particle cementation to occur.

Fig. 6.10(a) and Fig. 6.10(b) shows the variation of $r_{u,\,max}$ with the crude oil content for both treated and untreated specimens respectively at γ = 0.5% and 1.0% cyclic strains. The value of $r_{u,\,max}$ can be directly related to the liquefaction resistance of the corresponding specimen. At γ =0.5%, for untreated contaminated samples, the liquefaction resistance increases initially as the crude oil content increases. At ω = 4% crude oil content, the sample experienced maximum resistance against liquefaction. Again, on further increasing the crude oil content, the liquefaction resistance drops sharply and after $\omega \geq 8\%$ it becomes lower than the virgin sand.

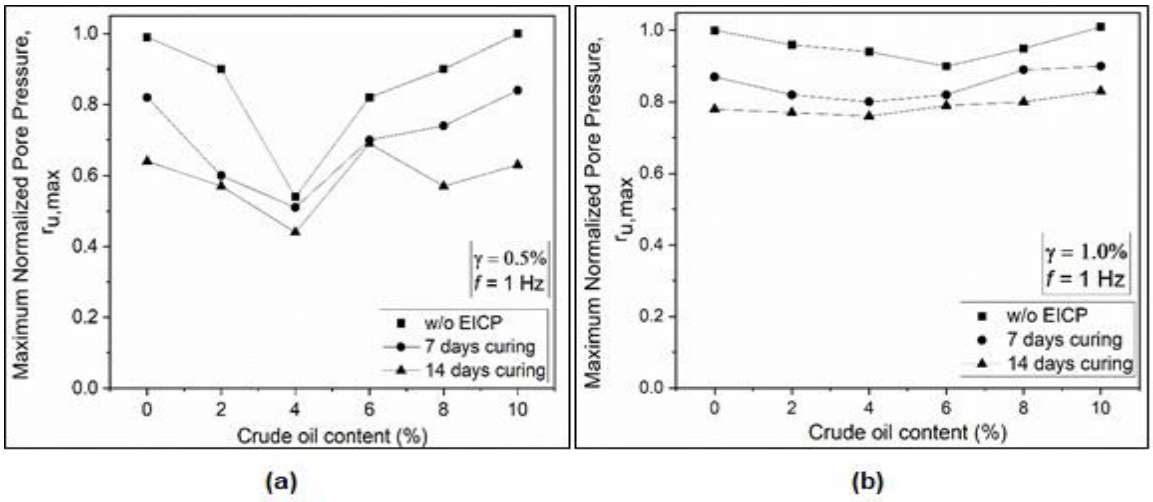

Fig. 6.10 Coupled effect of crude oil contamination and EICP treatment on maximum pore pressure ratio at (a) γ =0.5% and (b) γ =1.0%

Calcite precipitation improves the cyclic resistance of the oil contaminated samples owing to reduction in the $r_{u,\,max}$ values. The $r_{u,\,max}$ of treated specimens subjected to 7 days curing was 1.2-1.5 times their corresponding untreated ones. The improvement was significant at all oil contents except at ω = 4%. Also, for 14 days cured specimens, some inconsistencies were seen at ω = 4% and 6% which has been considered as the transition zone.

It is also worth noticing that the maximum gain in the cyclic resistance was attained within the first 7 days of curing. This observation is supported by the results presented in Table 6.1 obtained through the tube tests where the 96% of the calcite precipitation was achieved in first 7 days itself. The variation of $r_{u,\,max}$ of untreated samples with crude oil content at γ = 1.0% revealed that the maximum cyclic resistance was observed at ω= 6%. However, as discussed previously, then number of cycles required to initiate liquefaction was less for ω = 4%. Moreover, after EICP treatment, the specimens subjected to 7 days curing showed an indistinct transition zone between ω = 4% and ω = 6%. The effect of oil contamination was not prominent for 14 days cured specimens. The $r_{u,\,max}$ profile with the crude oil content was practically flat or constant. The $r_{u,\,max}$ of treated specimens subjected to

7 days curing was 1.12-1.2 times their corresponding untreated ones while for 14 days cured samples, this value lied in the range of 1.18-1.3.

In the preceding sections, the comparison between the cyclic strengths of the treated and untreated specimens have been made based on the maximum pore pressure ratio values attained during 100 loading cycles. This criterion was selected since some of the samples did not show any signs of liquefaction even after 300 to 400 loading cycles. However, to cater further justification to the inferences reported in the previous sections, cyclic resistance of treated and untreated sand in terms of the required number of loading cycles to reach liquefaction was calculated theoretically using an empirical model developed by Seed et al. (1975b). In this model, r_u is expressed as a function of the cycle ratio, which is the ratio of the number of applied uniform cycles of loading, N, to the number of cycles required to cause liquefaction in the soil, N_L, and an empirically determined parameter α as per eq. (6.2)

$$r_u = \frac{1}{2} + \frac{1}{\pi}\arcsin\left(2.\left(\frac{N}{N_L}\right)^{1/\alpha} - 1\right) \tag{6.2}$$

This equation was later simplified by Booker et al. (1976) as eq. (6.3)

$$r_u = \frac{2}{\pi} arcsin\left(\frac{N}{N_L}\right)^{1/2\alpha} \tag{6.3}$$

Equation (6.2) can further be utilized to calculate the number of loading cycles required to attain liquefaction, provided, the value of pore pressure ratio (r_u) reached, and the corresponding maximum number of loading cycles (N) considered in the study are known. For simplicity, the value of the empirical constant, α, has been taken as 0.7 (Polito et al., 2008; Porcino and Diano, 2016). Based on that, the variation of theoretically calculated N_L

with crude oil content for both treated and untreated specimens have been shown in Fig. 6.11. Fig. 6.11(a) suggests that at $\gamma = 0.5\%$, a distinct peak was observed at $\omega = 4\%$ for untreated samples. EICP treated samples showed a high number of N_L as compared to untreated ones. For $4\% \leq \omega \leq 6\%$, the change in N_L for treated samples was not significant, but further increase in ω resulted a remarkable reduction in N_L. There was a nearly two-fold increase in N_L from 361 for the untreated contaminated sample to 714 for 14 days cured sample at $\omega = 4\%$. Similarly, from Fig. 6.11(b), at $\gamma = 1.0\%$, N_L increases with increasing ω up to $\omega = 4\%$. For $4\% \leq \omega \leq 6\%$, the change in N_L was not significant but with further increase in ω, a remarkable reduction in N_L was observed. The value of N_L continues to drop thereafter up till $\omega = 10\%$. It can also be yet again noticed that the gain in the strength was more significant during the first seven days of curing. This observation was consistent at both cyclic strain values however, it was more pronounced at $\gamma = 1.0\%$.

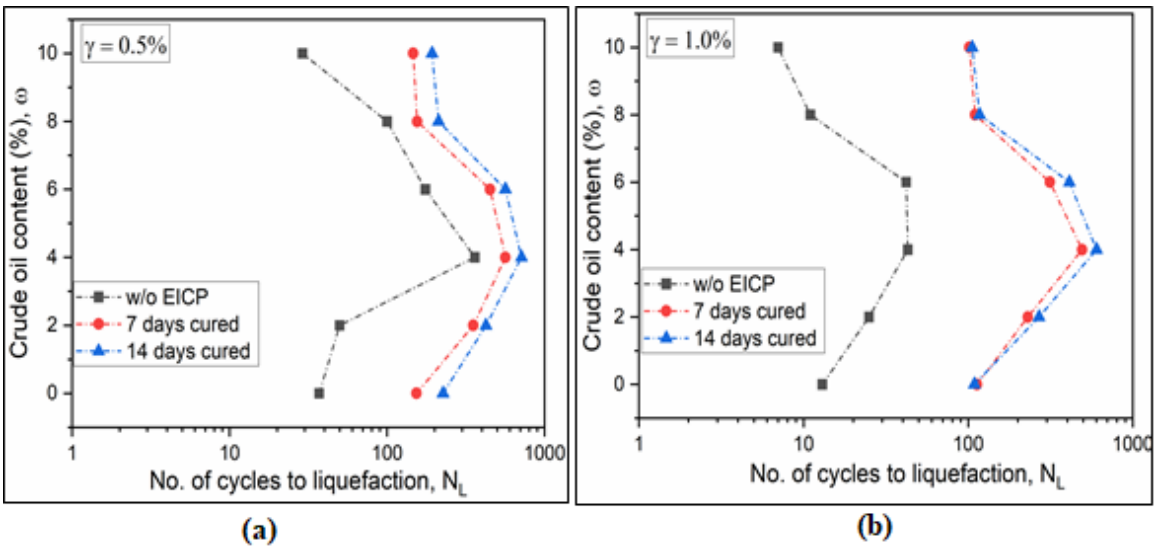

Fig. 6.11 Variation of theoretically calculated cycles to liquefaction with crude oil content at (a) $\gamma = 0.5\%$ and (b) $\gamma = 1.0\%$

6.3.3 Cyclic Secant Shear Modulus and Modulus Degradation curve

When fully saturated soils undergo cyclic loading in undrained conditions involving moderate to high cyclic shear strain amplitudes, γ, their stiffness and strength decreases with the number of cycles, N. Such a cyclic degradation is one of the most destructive and substantial soil dynamics phenomenon. Cyclic loadings may cause saturated sands to loose large portion of their initial stiffness and in extreme loadings they may completely lose their stiffness and liquefy. Therefore, cyclic shear modulus or cyclic stiffness (G_o) is an important parameter in liquefaction assessment of sands. In fact, several G_0 based liquefaction assessment charts are also in use to evaluate in-situ liquefaction potential of sands. Fig 6.12 shows the deviatoric stress versus shear strain results of the clean and contaminated Guwahati sand with and without EICP treatment for ω = 0%, 4% and 8% at γ = 0.5%. The slope of the line joining any point in the hysteresis loop to the origin of the stress strain diagram as shown in the Fig. 6.12 will give the value of cyclic secant shear modulus at that particular instance. The maximum value of secant shear modulus (G_{max}) was achieved at the point corresponding to maximum stress value (attained during the first loading cycle). It can be observed that the slope of the stress-strain curve of untreated sand is much smaller as compared to the EICP treated specimen. Similarly, Fig. 6.13 shows the deviatoric stress versus cyclic shear strain results of the clean and contaminated Guwahati sand before and after 14 days EICP treatment for ω = 0%, 4% and 8% at γ = 1.0%. The observed pattern was similar to those at 0.5% cyclic strains. Higher levels of deviatoric stresses were achieved for 1.0 % strain as compared to 0.5% cyclic shear strain. Also, there was a significant improvement in the stress levels after EICP treatment. Hence, it can be concluded that calcite precipitation causes a considerable increment in the G_{max} values.

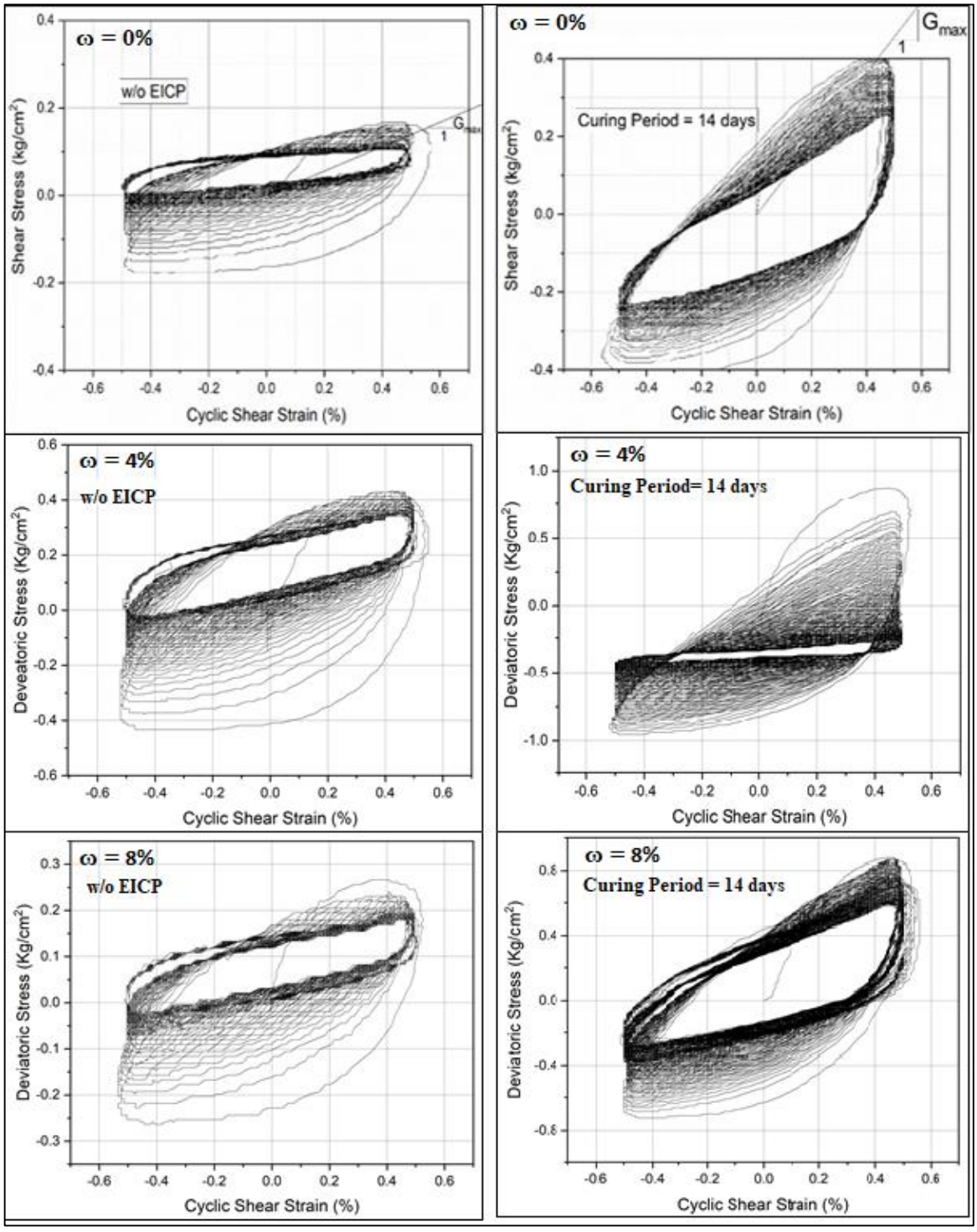

Fig. 6.12 Deviatoric stress versus cyclic shear strain profiles before and after EICP treatment for ω = 0%, 4% and 8% and γ =0.5%

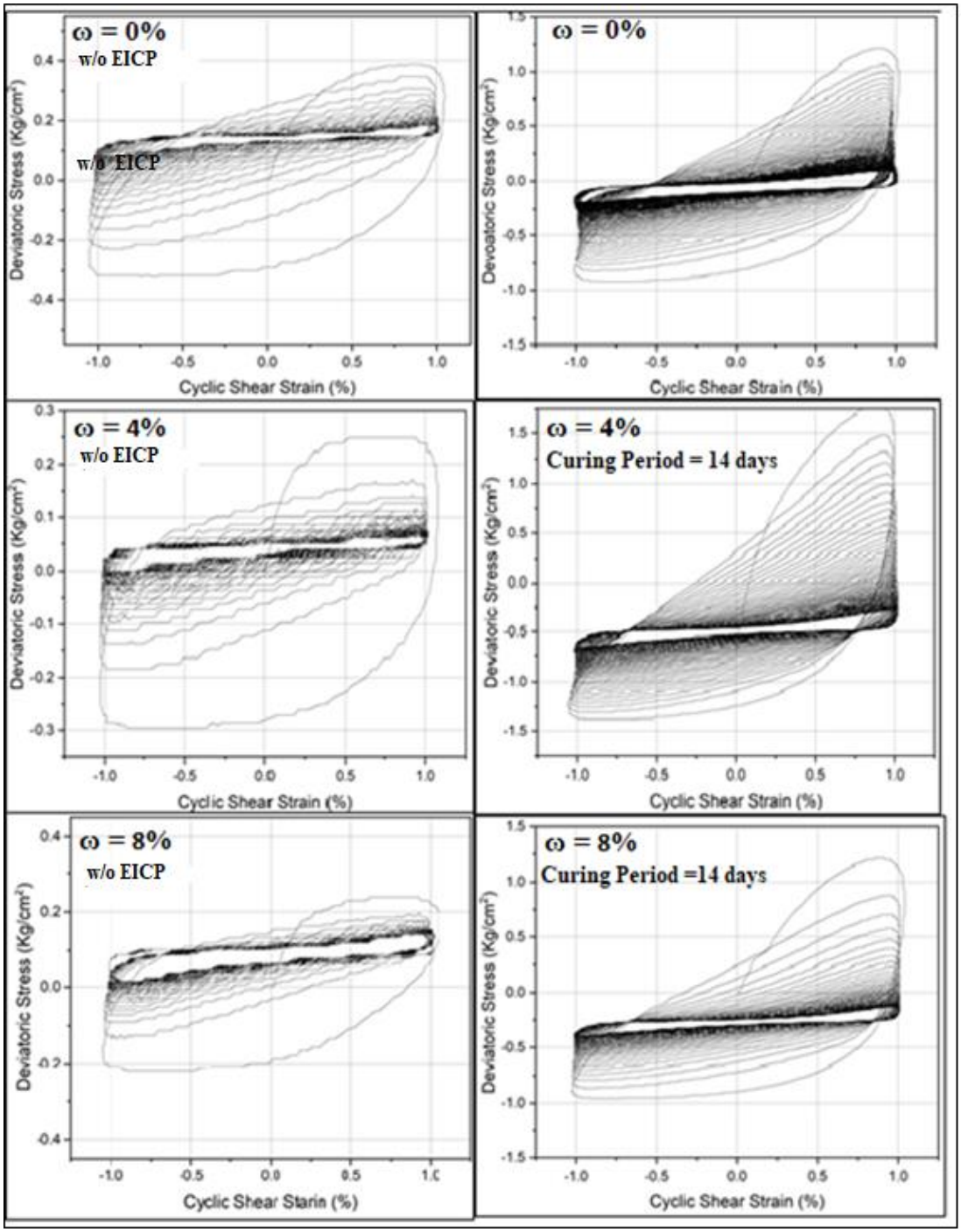

Fig. 6.13 Deviatoric stress versus cyclic shear strain profiles before and after EICP treatment for ω = 0%, 4% and 8% and γ =1.0%

Fig. 6.14 shows the coupled effect of crude oil content and EICP treatment on the G_{max} values of the Guwahati sand. The effect of crude oil contamination on the G_{max} is quite similar to the trend observed for $r_{u,\ max.}$ A well-defined transition point was observed at ω = 4% for

both γ= 0.5% and 1.0%. There was no significant change in the value of G_{max} after 8% and it was nearly constant. This observation was consistent with the studies conducted by Rajabi and Sharifipour (2017a). EICP treatment caused a substantial improvement in the G_{max} values of crude oil contaminated sand. A two-fold increase was witnessed in the G_{max} values of contaminated sand after 7 days of curing irrespective of the applied cyclic strain. However, in general, G_{max} values obtained at γ = 1.0% was smaller than those obtained at γ = 0.5%. It should also be noted that unlike in case of $r_{u,\,max}$, G_{max} for ω ≥ 6% (equal to for γ =1.0%) was found to be lower than the virgin sand for both untreated and treated sand. It implies that the negative effect of crude oil contamination on G_{max} was observable only when crude oil content exceeds 6%.

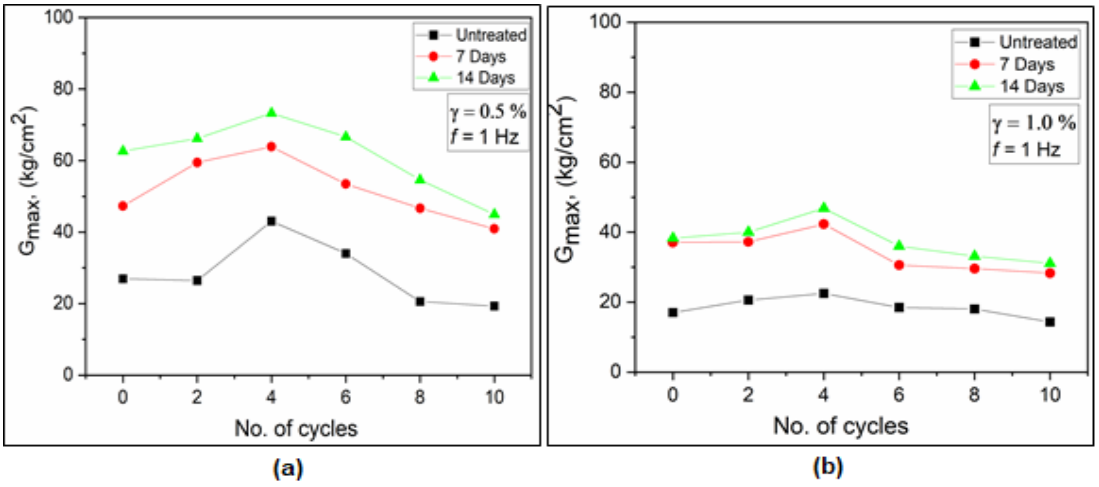

Fig. 6.14 Coupled effect of crude oil contamination and EICP treatment on G_{max} values at (a) γ =0.5% and (b) γ =1.0%

Whenever saturated sand is subjected to cyclic loadings, it causes generation of excess pore pressure. This excess pore pressure reduces the effective stress between the sand grains. Moreover, it is widely acknowledged that shear modulus is directly proportional to the effective stress (Hardin and Drnevich 1972). Hence, reduction in mean effective stress also causes reduction in the cyclic stiffness. This reduction in the cyclic secant modulus with

number of loading cycles has been termed as cyclic degradation. The declining slopes of the cyclic stress-strain loops in Fig. 6.12 demonstrate how the secant shear modulus at cycle N, $G_N = \frac{\tau_N}{\gamma}$, decreases with N. Here, τ_N = cyclic shear stress amplitude at cycle N. The reduction of G_N with N in the cyclic strain-controlled tests with constant γ is typically quantified by the degradation index, δ_N as per equation (6.4),

$$\delta_N = \frac{G_N}{G_{max}} = \frac{\tau_N/\gamma}{\tau_1/\gamma} = \frac{\tau_N}{\tau_1} \tag{6.4}$$

The variation of δ_N with N for untreated and treated sand is shown in Fig. 6.14, Fig. 6.15 and Fig. 6.16. Idriss et al. (1972) introduced a term called degradation parameter, *t*, which is defined as per equation (6.5),

$$t = -\frac{\log \delta_N}{\log N} \tag{6.5}$$

It quantifies the rate of degradation of the shear modulus with the number of cycles due to pore pressure build up. Negative sign is indicative of reduction of G_N with N. The characterization of degradation through *t* parameter is typically done for clays because plot of $\log \delta_N$ versus $\log N$ is a straight line or clays. However, an approximate analysis of degradation with *t* parameter can also be made for sands. Each figure along with the degradation curves, also shows the equation of a linearly fitted straight line on their respective $\log \delta_N$- $\log N$ plot. The value of the slopes for each equation gives the rate of modulus degradation of its respective plot.

Fig 6.15 shows the effect of crude oil content on the modulus degradation curves of Guwahati sand. Since the applied cyclic shear strains are larger than 0.15%, the cyclic pore water pressure starts building up from the very first cycle of cyclic shearing causing continuous reduction of G_N and associated δ_N.

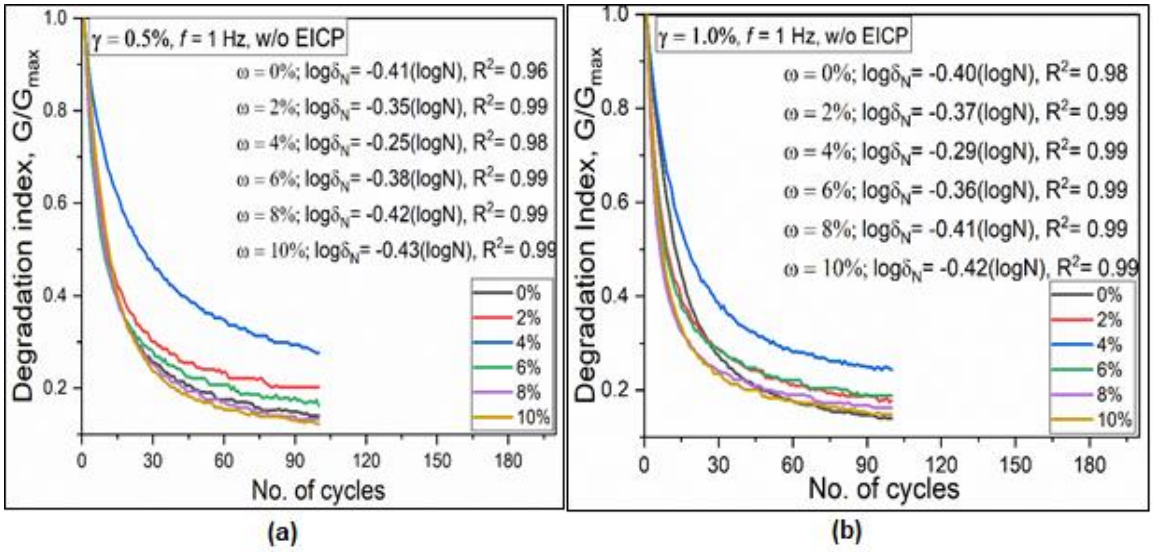

Fig. 6.15 Variation of degradation index, δ_N, with the number of cycles. N, and the degradation parameter, t, for untreated contaminated specimens at (a) γ = 0.5% and (b) γ = 1.0%

The *t* parameter has been approximated over the range of 1000 loading cycles. In the initial 5-8 cycles, the crude oil contaminated sand cyclically degrades at a faster rate than the uncontaminated sand. This rate increased with increasing crude oil content. The average rate of cyclic degradation approximated over the entire range of loading cycles decreases up to ω = 4%. Beyond this point, the *t* parameter showed an increasing trend with increasing oil content up to ω = 10%. This observed pattern was strongly supported by the excess pore pressure results shown in Fig 6.6.

EICP enhanced specimens showed a remarkable improvement in the degradation rate of G_N. Fig. 6.16 and Fig. 6.17 presents the degradation curve of oil contaminated specimens after EICP treatment at γ = 0.5% and γ = 1.0% respectively. When 14 days cured samples were cyclically sheared at γ =0.5%, the degradation parameter, *t*, was reduced by 80-85%.

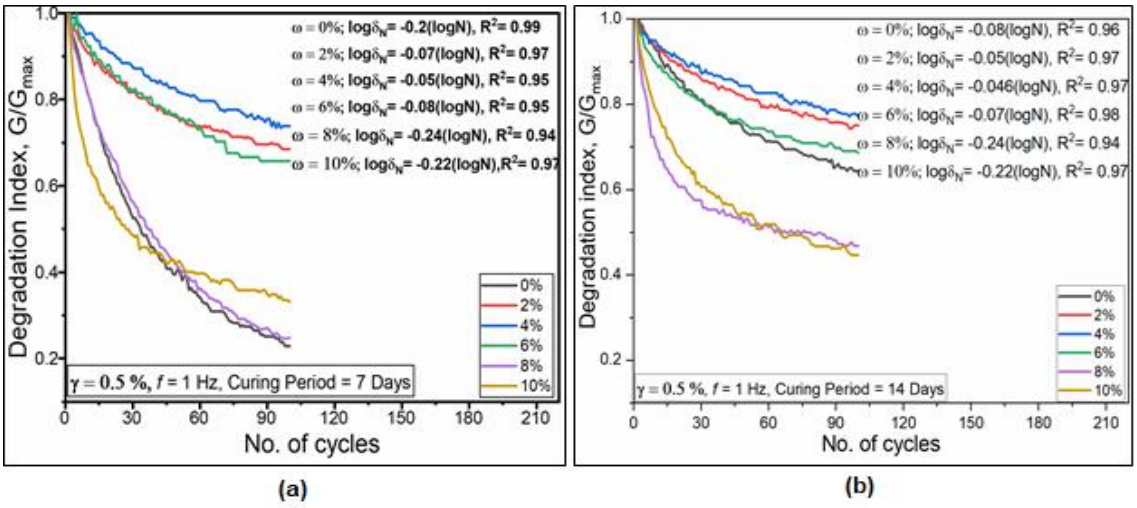

Fig. 6.16 Variation of degradation index, δ_N, with the number of cycles. N, and the degradation parameter, t, for EICP treated specimens at γ = 0.5% for (a) 7 days and (b) 14 days curing

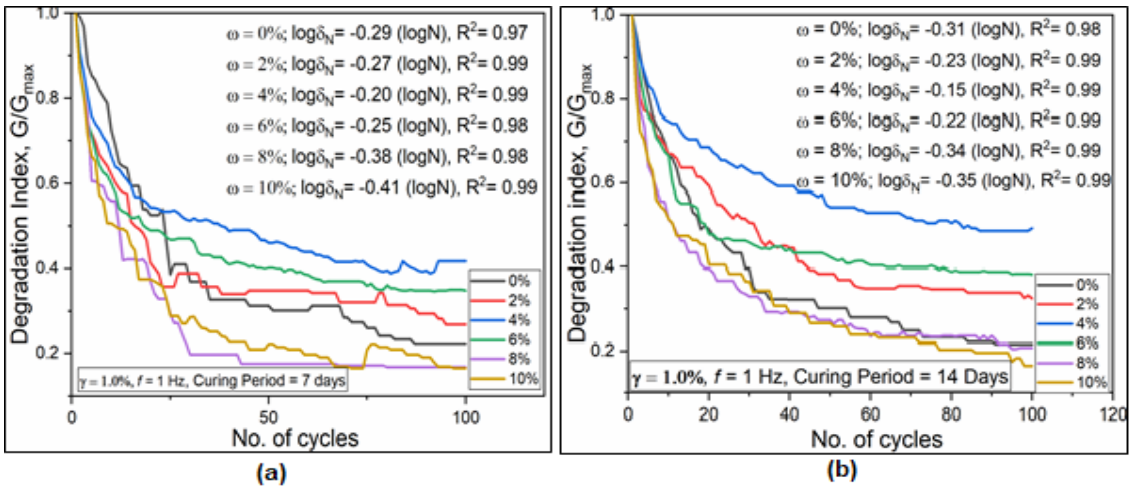

Fig. 6.17 Variation of degradation index, δ_N, with the number of cycles. N, and the degradation parameter, t, for EICP treated specimens at γ = 1.0% for (a) 7 days and (b) 14 days curing

For ω = 8% and 10%, the observed reduction was 65% and 62% respectively in view with the fact that the efficiency of EICP treatment decreases with increasing oil content. In case when γ =1.0%, the reduction in the degradation rate after 14 days curing period carried over a wide range of 28% for ω = 0% to 38.8% for ω = 6%. While for ω = 8% and 10% this value

was observed to be 17.07% and 16.6% respectively. It can be noticed that decrease in *t* parameter after 14 days treatment was more in case of $\gamma = 0.5\%$ as compared to $\gamma = 1.0\%$. Hence it again implies that the EICP treatment is more efficient at lower strain levels.

6.4 Summary

This study has shown that EICP could effectively improve the cyclic behavior of crude oil contaminated Guwahati sand. The effect of crude oil contamination on the liquefaction behavior of Guwahati sand has been discussed in prior. Initial oil contamination moderately increases the cyclic resistance. Soon after reaching the transition point i.e. $\omega = 4\%$, the cyclic resistance falls off drastically. The effect of constituent chemicals on calcite precipitation ratio has also been discussed which determined 1M urea, 0.67M $CaCl_2$ in the ratio of 1:1.5 and 5g/L of enzyme as the concentration yielding maximum precipitation efficiency. An extensive examination evaluating the effect of EICP treatment on the generation of excess pore pressure and stiffness degradation at various crude oil contents, curing periods and cyclic shear strains has been conducted. The efficiency of EICP was reduced at higher degrees of contamination due to the reduced enzyme activity and particle roughness. Around 96% of total precipitation was achieved during 7 days of curing itself. A two-fold increase in the G_{max} value was observed for 7 days cured specimens. Moreover, the stiffness degradation parameter was reduced upto 80% at $\gamma = 0.5\%$. The observed patterns of the excess pore pressure levels and degradation parameters at two different cyclic strains indicates that the efficiency of the EICP treatment diminish at higher strain levels. The observed results have been supported by the SEM analysis in order to elucidate the effects of microscopic alterations leading to changes in macroscopic behavior.